





# A Unified Sensor Platform for Investigating Corona Effects on Overhead Lines

## Journal Article

### Author(s):

Bleuler, Pascal ; Polonelli, Tommaso ; Xiao, Yu; Stadler, Benjamin; Gallina, Lorenz; Kirchner, Hannah; Magno, Michele ; Franck, Christian 

### Publication date:

2023

### Permanent link:

<https://doi.org/10.3929/ethz-b-000630834>

### Rights / license:

[In Copyright - Non-Commercial Use Permitted](#)

### Originally published in:

IEEE Transactions on Instrumentation and Measurement 72, <https://doi.org/10.1109/tim.2023.3312702>

### Funding acknowledgement:

187087 - AeroSense: a novel MEMS-based surface pressure and acoustic IoT measurement system for wind turbines (SNF)

# A Unified Sensor Platform for Investigating Corona Effects on Overhead Lines

Pascal Bleuler, Tommaso Polonelli, *Member, IEEE*, Yu Xiao, Benjamin Stadler, Lorenz Gallina, Hannah Kirchner, Michele Magno, *Senior Member, IEEE*, Christian M. Franck, *Senior Member, IEEE*

**Abstract**—Outdoor long-term continuous measurements of overhead conductor corona are needed to better plan high-voltage power grids. Most of the time, only single aspects of corona are being measured over short periods of time in controlled environments using complex and expensive sensors. This paper presents a single unified wireless sensor platform to reliably measure three distinct corona-related quantities on high-voltage lines. Namely, the corona current through the line, the ground-level electric field, and the ground-level ion current density. The platform is a distributed, cost-effective, low-power IoT system that enables outdoor measurements of lines exposed to real weather over extended periods of time allowing to highlight correlations across seasons. With example measurements, the importance of having heterogeneous sensors measuring different corona effects in a unified way is demonstrated. The corona current sensor is shown to operate at up to hundreds of kV while still providing an accuracy of 83 nA and average power consumption of 1 mW. Corona effects, collected every 4 s with a sampling frequency up to 1 kHz, make it possible to visualise correlations with environmental parameters such as humidity, precipitation, and wind speed in novel ways through on-board processing of the collected data.

**Index Terms**—IoT, Corona, Grid, Energy, Low power.

## I. INTRODUCTION

A successful energy transition requires the integration of renewable power sources into our electricity grids. Today's grids, designed for centralized and predictable power production, lack the capacity to absorb the widely distributed and intermittent outputs expected from renewables. To augment grid capacity, new overhead lines need to be built, or existing ones upgraded to higher voltages. In recent years, the Internet of Things (IoT) has pushed technology of distributed and long-term grid analysis forward thanks to inexpensive and low-power wireless sensor nodes [1], [2]. A major design parameter in the planning of overhead lines is the so-called corona effect. Since those effects depend on weather and other atmospheric conditions and geographic specificities, a large-scale deployment of sensors is desirable to monitor the grid over months or years [3].

High voltage overhead lines are commonly used to transport electrical energy over large distances. Metallic conductors above the earth's surface are galvanically insulated from ground potential through the surrounding air and the insulators by which they are mechanically attached to supporting towers. Conductors can be seen as cylinders above ground in the vicinity of which the electric field is quasi-uniform on the length scale of a fraction of a radius. But when small protrusions, such as water droplets deposited through rain or environmental

particles sticking, appear on the conductor surface, the field is locally increased. If this increase rises above the critical electric field strength of the insulating medium (in this case, the surrounding air), a partial discharge occurs in which a small portion of the gas is ionized [4].

A Partial Discharge (PD) is a kind of electrical discharge that, unlike a breakdown, does not bridge the full gap between the two electrodes (in this case, the overhead conductor and ground). When such a discharge happens in a gas, it is called corona [5] and secondary phenomena caused by corona are called corona effects. These effects are highly dependent on environmental conditions and thus, corona should ideally be measured out in the field under real conditions. Traditional partial discharge measurement involves large coupling capacitors and other kinds of equipment that can be expensive and/or impractical for long-term outdoor measurements [5], [6]. Moreover, the limiting factors in overhead lines are generally not the discharges themselves, but the corona effects they cause [5]. Those include acoustic noise emissions due to the local and sudden heating of the air, radio interference, ozone formation, and others. Corona effects can thus not be measured using a single sensing element, and require a heterogeneous set of devices to cover the whole spectrum of physical phenomena that they imply.

Several widely used and available empirical formulas exist, that for a given conductor bundle geometry and a calculated electric field value on the conductor surface, predict audible noise emissions for both AC and DC lines [7], [8]. While many factors other than bundle geometry and operating voltage influence corona performance, such as conductor surface; it is atmospheric conditions, depending on both the environment and the weather, that probably have the highest and most dynamic variability during the operating lifetime of a line. Environmental parameters include parameters such as the altitude and pollution of the surroundings. As for the weather, rain is the main factor, but other types of precipitation, humidity, wind, etc., also play an important role. Some of these common formulas can be adjusted to account for parameters such as altitude [7], [8] or rain rate [9] in the hope of increasing their predictive power. However, as noted by their authors themselves, those formulas should preferably be used in conjunction with actual long-term measurements of lines similar in design (bundle geometry and conductor materials) located in "similar climatic conditions" [7]. Regarding rain rate, attempts have been made to infer long-term results from short-term measurements, but they come with limitations, such as the need for the conductor to be completely wet to be

valid [10].

Historic measurements reported in literature are limited to very specific geographic regions and conditions particular to that time and place. In fact, a large majority come from either test sites either in Oregon [11] or Montreal [12]. Moreover, they date back to half a century ago and are limited by the technology of their time. For instance, while [6] presents a setup capable of measuring both the corona loss current and the radio interference caused by corona, it shows the huge complexity involved in such an endeavor, including Frequency Modulation (FM) transmitters, fiber optics connections carrying analog signals, and magnetic tape recorders. In recent years there has been a rekindled interest in new continuous long-term measurement campaigns in outdoor settings [13], [14], that would be facilitated by heterogeneous and distributed sensor platforms able to collect data of corona-related quantities. In this context, IoT technologies provide several advantages over techniques traditionally used in high-voltage engineering thanks to typical features like cost-effectiveness, wireless connectivity, and optimized energy consumption that allows months or even years of operation with a single battery charge.

In the past, corona effects and related quantities have mainly been measured separately in isolated sporadic experiments [4], [8], [15]–[17]. In none of the cited works from the literature a distributed low-power acquisition system of heterogeneous sensors working on the same unified platform has been used. Hence, in this work, we propose an innovative sensor platform leveraging IoT technologies, reliably enabling continuous measurements of three different physical quantities, while keeping energy requirements to extremely low levels. This platform is used to monitor: (i) the corona current through the line, (ii) the ground level electric field, (iii) and the ground level ion current density, through a network of heterogeneous wireless sensor nodes, where all of them are connected to a single gateway hub collecting data in a unified way. Our sensor platform's reduced cost and low energy consumption, coupled with its usability, flexibility, and reliability, make the continuous long-term monitoring of several distinct corona effects concurrently at the scale of entire girds feasible.

This paper introduces a practical tool for monitoring corona performance in an easy-to-deploy and affordable way over long periods. Proof of concept measurements are presented, demonstrating the platform's performance and advantages using two application scenarios. First, the concurrent measurement of different corona quantities is used to compare the corona behavior of two different HVDC overhead line conductors in the laboratory. Then, correlations with weather conditions are shown on an outdoor HVDC test line with novel visualization techniques, taking advantage of onboard processing, to deal with highly dynamic signals. The main contributions of the paper are to: (i) design and implement a modular sensor platform that uses a smart data flow with low-power wireless communication and onboard processing; only the relevant features are transmitted to the gateway through a Bluetooth Low Energy 4.1 (BLE) link; its power consumption is as low as 1 mW in average, (ii) show the platform's capability to discriminate the corona performance of different high voltage overhead line conductors using all

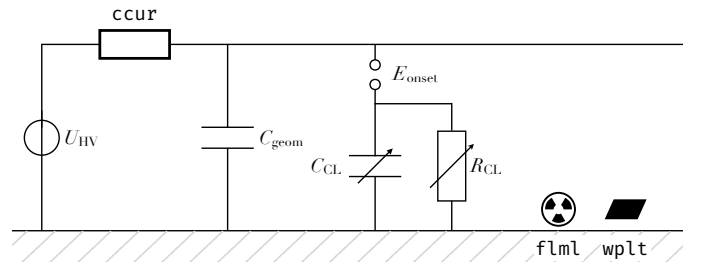


Fig. 1. Simplified lumped element model of an HVDC test line that can be subjected to corona effects based on descriptions in [18], [19]. The sensors denoted in monospaced font `ccur`, `flml`, and `wplt` are explained later in this paper. With no corona discharge, the overhead line is a simple capacitance towards ground  $C_{\text{geom}}$  dependent on its geometry (for a simple cylinder above perfect ground  $C_{\text{geom}} = \frac{2\pi l \epsilon}{\cosh^{-1}(h/r)}$ , [20]) and connected to a high voltage source  $U_{\text{HV}}$ . The spark gap marked  $E_{\text{onset}}$  remains open. When the electric field  $E$  somewhere around the line is sufficient for corona to occur,  $E > E_{\text{onset}}$  and space charges flow through  $C_{\text{CL}}$  and  $R_{\text{CL}}$ .

three measured quantities, (iii) demonstrate the possibility to measure corona loss currents with 83 nA accuracy and ion currents at ground level with 10 nA accuracy both using only inexpensive and commercial components, and (iv) exploit the platform's onboard processing capabilities to enable novel visualizations of corona data that is useful for the analysis of long-term measurements, correlating corona behavior with environmental parameters, such as wind speed, humidity, and precipitations.

## II. BACKGROUND

### A. Corona effects around overhead lines

In Fig. 1 (ignoring, for now, the sensors `ccur`, `flml` and `wplt` denoted with monospaced font), a high voltage source  $U_{\text{HV}}$  is connected to an overhead line conductor that has a parasitic capacitance towards the ground due to its geometry  $C_{\text{geom}}$ . In normal operating conditions, nothing else is connected to the high-voltage source. The test line is unloaded and the leakage currents through the insulators holding the line are neglected (i.e., the resistance of the insulators toward the ground is considered infinite).

Corona discharges can occur anywhere on the line where the electric field  $E$  is subjected to local disturbances such that  $E$  exceeds the so-called corona onset value  $E_{\text{onset}}$ . In the simplified schematic of Fig. 1, those discharges are modeled by the spark gap marked  $E_{\text{onset}}$  that is open as long as  $E < E_{\text{onset}}$  and closes when  $E \geq E_{\text{onset}}$ . The generated space charge will modify the parasitic capacitance of the line as modeled by  $C_{\text{CL}}$ , and those space charges that flow towards the ground will count as ohmic losses through  $R_{\text{CL}}$ .

### B. Corona-related quantities around HVDC test lines

Historically, High Voltage Alternating Current (HVAC) technologies have dominated the energy transmission landscape primarily due to the transformer that only works with alternating currents. However, the advent of thyristors valves in the 1970s and later insulated-gate bipolar transistor (IGBT) valves in the 1980s led the way to more High Voltage Direct Current (HVDC) connections, which have many advantages

over HVAC links [21]. In these circumstances, the total or partial conversion of an HVAC line to a fully HVDC [22] or hybrid HVAC/HVDC line where multiple systems share the same right of way or towers [14] are considered or even under construction [22]. This trend toward HVDC transmission lines is one of the forces behind new research efforts in corona effects around overhead lines. Moreover, to ensure public acceptance and to comply with local regulations, audible noise emissions caused by corona discharges have increasingly become a topic of interest in recent years. Below, we list three electrical corona-related quantities that are particularly relevant in this context.

The first two directly relate to the electromagnetic environment around HVDC overhead lines. It is defined by the electric field strength ( $|\vec{E}|$ ), the ion current density ( $\vec{J}$ ) and the space charge density ( $\rho$ ) [23]. Indeed, in a DC field, the free charge carriers created by corona discharges will not recombine at the next half-wave as they do in AC but flow along field lines. This charge flow is the current passing through  $R_{CL}$  when  $E \geq E_{onset}$  in the simplified model of Fig. 1. It can be measured as an ion current density at ground level. Furthermore, the changing space charge environment caused by the corona will also impact the electric field strength at ground level.

As test lines are unloaded, they only carry the corona current. This current corresponds to that of all the free charge carriers caused by all the discharges happening along the line, and can be measured as the series current occurring between the high-voltage source and the overhead line itself.

The first two of those quantities are directly interdependent and localized. In Fig. 1,  $w_{plt}$  and  $f_{lml}$  measure the ground level ion current density using a Wilson plate, and the electric field at ground level using a field mill at the specific position where the respective sensors are placed. A modular sensor platform would allow a large number of those sensors to be measuring concurrently at several locations.

The corona current is measured by the shunt resistor  $c_{cur}$  through which all the current supplied to the entire test line flows, and is placed after the high voltage source  $U_{HV}$ . Being placed on high potential, it has to be galvanically isolated from ground.

### III. OUR SENSOR PLATFORM

#### A. Platform architecture

The proposed design is a modular device using STMicroelectronics' STWIN SensorTile as its core. External circuitry targets the acquisition of specific physical parameters, i.e., highly accurate corona current measurements, electric field measurements, or ion currents at ground level through Wilson plates. Such an architecture enables us to rapidly deploy a large number of different sensors. Having a single receiver hub recording data from multiple devices that use the same sensor nodes as a common platform being of great benefit.

The SensorTile has an STMicroelectronics STM32L4R9, a 120 MHz ARM Cortex-M4 MCU with 2 MB of internal RAM. An STBC02 battery manager is included, along with a digital absolute pressure sensor (LPS22HH), a relative humidity and

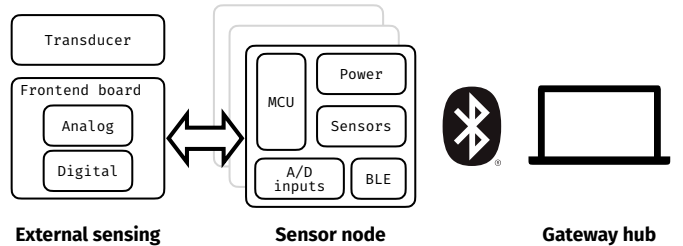


Fig. 2. Schematic representation of our sensor platform architecture. Each node of the system is based on the STMicroelectronics' STWIN SensorTile. The nodes have internal sensors but can also be expanded by any combination of external sensing transducers and custom-made analog and/or digital frontends PCB. The physical link between nodes and external elements provides a programmable interface and auxiliary power. The node's MCU processes the data and sends it out wirelessly over BLE to the gateway hub. The latter includes a workstation that locally stores and processes the collected packets from one or several nodes in parallel.

temperature sensor (HTS221), and two wideband MEMS microphones.

The sensing is either performed by these onboard sensors on the node itself, on external PCBs (frontends), and/or more substantial pieces of external hardware. Depending on the sensor and the nature of the measured quantity, the signal is digitized either on the fronted PCB or using the MCU's internal ADCs. A 40-pin flex connector and a 12-pin female header on the SensorTile enable this modularity.

#### B. Corona effects sensors

1) *Corona current*: On a test line with the geometries we are interested in, corona currents are in the  $\mu\text{A}$  to  $\text{mA}$  range. With our test line and our environmental conditions, variations in HVDC corona levels during fair weather appear to be within a much smaller range than those observed during rain. This dictates the need for a sensor with a large dynamic range. In hybrid setups such as those described in II-B, the DC corona current can sometimes not be distinguished from an AC component much larger than it. Here again, a high dynamic range is required to ensure that the signal is fully captured with a measurement accuracy to discriminate the corona current from the parasitic capacitive current due to the electrode geometry ( $C_{geom}$  in Fig. 1).

Recent research into corona current sensors has had an emphasis on resolving individual discharge pulses and efforts were thus concentrated on reaching bandwidth higher than the MHz [15]. On the other hand, we are solely interested in the low-frequency component of the corona current, resulting from the drift of free charge carriers in the DC electric field.

To measure this high dynamic range low bandwidth signal, we designed a specific frontend board with a differential current sense amplifier and a high-resolution ADC (24-bit). The acquisition chain comprises a fully differential analog circuit that minimizes noise, temperature dependencies, and component aging. A cascade of two low-pass filters (LPF) with a cut-off frequency of 200 Hz is imposed before and after the differential amplifier: A passive first order LPF to reduce differential noise before amplification and an active second order LPF to counter aliasing effects in the digitization. The



amplification stage relies on the Texas Instruments INA186, a low-power bidirectional, zero-drift, current-sense amplifier. It features a noise density of  $75 \text{ nV}/\sqrt{\text{Hz}}$  and a rail-to-rail dynamic range. The signal is digitized by a 24-bit ADC (ADS122U04) and sent over UART to the STM32L4R9 via the 12-pin female header.

Working on high potential conductors, the common mode at the INA186 input could generate measurement and electrical issues, such as internal partial discharges due to drastic voltage and electromagnetic field fluctuations. Thus, the common ground of the analog fronted and the negative INA186 input are clamped to the high voltage line through an ESD-rated capacitor and a  $\text{M}\Omega$  resistor. Moreover, all the input stages are protected up to 15 kV of ESD discharges.

The sensor is calibrated using a Keysight B2902A current source as a reference to supply a constant current. Three different configurations, from 1 to 3 in Table I, are available depending on the required current range and accuracy. While those have to be manually selected, one could easily imagine a dynamic switching if needed.

For the calibration a linear approximation is made to compensate for offset, gain, and temperature noise sources. Each range was calibrated at different points. Every 4 seconds, the sensor takes 100 measurements with a sampling frequency of 1000 Hz. Then the sensor calculates locally the mean over 100 measurements. This means a single BLE packet is sent and received every 4 seconds between the node and the gateway. The firmware flowchart is in Fig. 3, where low power states and error handling are supported. Each calibration was conducted for 15 minutes, resulting in 225 received values, representing the mean of over 100 current measurements. Moreover, the sensor was tested at different temperature points to quantify the temperature behavior. With the Keysight B2902A, the same current was generated as in the calibration process. The sensor was mounted inside a box and the same current was measured at three different temperatures. The battery stayed at room temperature. The frontend PCBs temperature sensor was used, and the resulting curve was normalized to calculate the correction factor.

As described in Table I, the corona current sensor can measure within a range of  $\pm 0.5 \text{ mA}$  with an accuracy down to  $83 \text{ nA}$  with a shunt resistor of  $33 \Omega$  (configuration 3).

2) *Ground level electrical field*: To measure the electrical field at ground level below an HVDC overhead line, field meters using the field-induced charge principle of the “vibrating element” or “field mill” types are generally used [23]. While other measurement principles, such as MEMS or optical sensors leveraging the Pockels effect are being investigated,

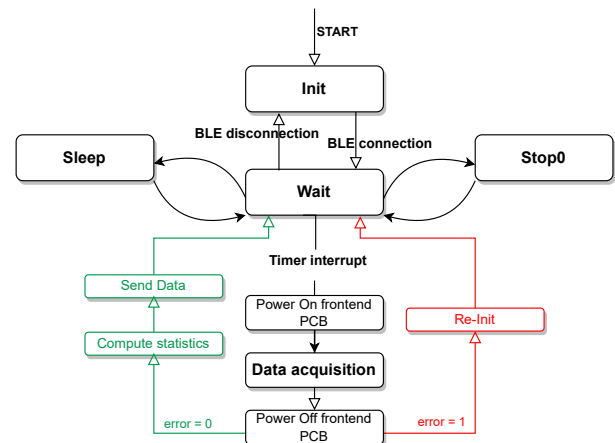


Fig. 3. Corona current sensor: firmware flowchart. *Stop0* indicates the lowest power consumption state, in which the node is completely off and not connected to the BLE. *Sleep* indicates a CPU inactivity, while the *Send Data* block includes the BLE transmission and the data serialization. The error handling includes the possibility of recovering from software/hardware faults caused by external electromagnetic noise (generated by the HV line) and environmental conditions, like humidity or water condensation inside the sensor enclosure.

they are not yet ideally suited for applications in a charge-rich environment or under hybrid AC/DC stresses, such as those of interest to us [24].

In our setup, we used field mill devices developed by Cui et al. at the Beihang University as described in [25]. A feature of interest of those specific field mills is their claimed weather resistance. While a known technique to avoid water ingress into field mills during rain is to use them upside down [26], this is not always practical and might not be sufficient to operate non-weather sealed field mills outdoors for long periods.

The output signal of the field mills is an analog voltage that fits the capabilities of the node MCU’s internal ADC. The signal is sampled at 10 kHz and 2000 points are acquired during each measurement. The mean, maximum and minimum values are processed on the MCU before being sent to the gateway every 2 seconds.

3) *Ground level ion current*: The ion current density at ground level is determined by measuring the current through a collecting plate electrode, slightly raised and insulated from the ground. Dividing this current by the plate surface yields the ion current density. This principle, called the Wilson plate, was initially developed for atmospheric currents [27] and has since been widely used in corona research around HVDC overhead lines [28]. The currents are usually in the nA to low  $\mu\text{A}$  range and have historically been measured by electrometers due to the low voltage between the plate and ground. In recent years, current-to-voltage op amp techniques with low input burden voltage have been used [28].

Our Wilson plate has a collecting surface area of  $0.49 \text{ m}^2$ . A frontend sensor amplifies the small DC output current of the Wilson plate to a voltage that can be digitized by the internal ADC of the STM32L4R9. This is achieved by first dropping the output current over a shunt resistance  $R_{\text{shunt}}$ . Notably, this resistance is adjustable by the user via onboard

TABLE I  
CORONA CURRENT SENSOR: CONFIGURATION, RANGE AND MEASURED DC ACCURACY

Configuration	Shunt resistor	Current range	Accuracy
-	$\Omega$	mA	$\mu\text{A}$
1	0.68	$\pm 24.0$	4.66
2	1.5	$\pm 10.0$	1.92
3	33.0	$\pm 0.5$	0.083

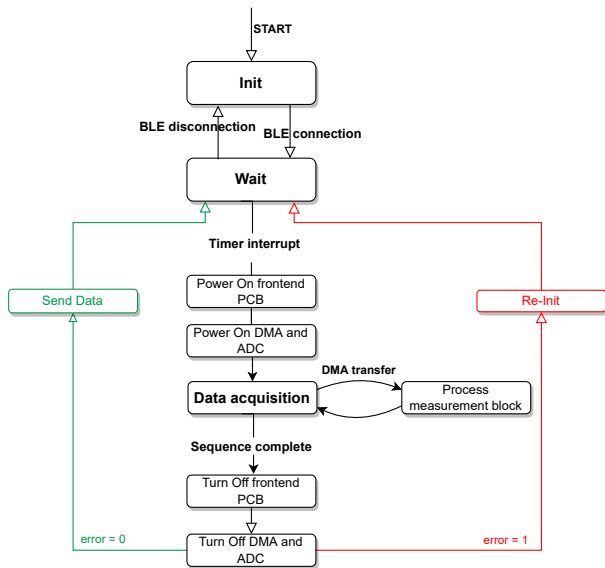


Fig. 4. Ground level ion current sensor: firmware flowchart. Error handling includes skipping faulty measurement blocks or sequences, system reset after unrecoverable errors or too many faulty measurement blocks or sequences or warnings, as well as logging to flash.

switches to account for different test line setups, allowing to read from 3.5 nA to 0.5 mA (maximum input current). After being passively low-pass filtered, the resulting voltage is amplified with a Maxim Integrated MAX4208, an ultra-low offset/drift precision instrumentation amplifier with a voltage reference buffer. By providing an offset voltage  $V_{\text{offset}}$  with the DAC of the STM32L4R9, the input range can be shifted to allow reading negative currents. To attenuate the noise from the amplifier, the signal is passed through a second passive LPF before being outputted to the STWIN.

The firmware periodically executes a measurement sequence: first, the frontend sensor is powered on, then the ADC and Direct Memory Access (DMA). After each DMA transfer, statistics are computed from the collected raw measurement data buffer. Once the desired amount of measurement blocks are collected, the frontend sensor is turned off, and the BLE characteristics are updated with the aggregated statistics. See Fig. 4 for the firmware flowchart.

Calibration is performed with a Keysight B2902A current source. For each configuration consisting of the tuple  $(R_{\text{shunt}}, V_{\text{offset}})$ , a linear approximation is made. Table II shows a selection of configurations. To account for changes on the STWIN side, the ADC is calibrated at each power cycle of the frontend board and the analog reference voltage is periodically measured.

### C. Wireless data transmission

To monitor corona activity over extended periods, we require sensor nodes to be low-power but do not need a high data throughput. As the main goal is to have a proof-of-concept sensing system to collect data in the university laboratories, the range over which data must be transmitted from nodes to the receiver hub is dictated by the overhead line geometry

and does not exceed a few tens of meters. These technical considerations, combined with the availability, price, and prior experience, made us opt for BLE to transfer data from nodes to the receiver gateway.

The SensorTile is equipped with a BlueNRG-M2 BLE 4.2 module on the node side. The firmware is based upon STMicroelectronics's example project BLE\_SampleApp contained within the STSW-STWINKT01 firmware package. In a peripheral role, the node advertises its characteristics and updates them with new data at predefined intervals.

The receiver gateway hub is a standard workstation that uses Nordic Semiconductor's nRF52840 dongle as its Bluetooth Low Energy interface. The receiver software is written in Python and uses Thomas Gerstenberg's blatann and Nordic Semiconductor's pc-ble-driver-py libraries among others. One receiver can connect to several nodes and subscribes to their characteristics.

The BLE connection was evaluated with multiple connected devices, up to 8, to check the real bandwidth supported by our hub. The main parameter that affects the connection speed in a BLE star network is the connection interval, which should be scaled so that the nRF52840 can communicate with all devices once within a certain period. The default time window, where the hub actively exchanges packets with a peripheral, corresponds to 7.5 ms. In that case, the optimal connection interval can be calculated for achieving the highest throughput. This corresponds to  $(7.5 \text{ ms} \cdot n_{\text{peripherals}})$ . To evaluate the BLE network throughput, we mainly focused on the notification rate and the number of packets transmitted per connection event, considering packets with 20 B of payload. Results are reported in Table III by varying the rate at which each peripheral is notifying the central and the number of connected devices. In the worst case, with 8 connected peripherals, we measured an average number of notifications per connection interval between 3 and 5, depending on the connection quality and peripheral-hub distance. Thus, in the worst case, our BLE network can support a throughput between 64 kbps and 106 kbps, while in the best scenario, with one device connected, it reaches 150 kbps.

### D. Power Consumption Characterisation

A power consumption analysis of the platform is performed with a Keysight N6705C DC Power Analyzer. The analysis is targeted on the corona current sensor programmed with the firmware described in Fig. 4.

In the *initial stage*, the platform is broadcasting and waiting for a BLE connection. In this part, the MCU runs in a

TABLE II  
GROUND LEVEL ION CURRENT SENSOR: CONFIGURATION, RANGE, AND ACCURACY

Config	$R_{\text{shunt}}$ k $\Omega$	$V_{\text{offset}}$ V	Current Range $\mu\text{A}$	Accuracy nA
C	4.59	1.34	$\pm 1.0$	7.0
D	0.232	1.34	$\pm 20.0$	69.0
Y	2.56	1.93	[-2.6, 1.0]	9.7
Z	2.56	0.375	[-0.5, 3.0]	10.0

TABLE III  
MAXIMUM NOTIFICATION RATE SUPPORTED VS. # PERIPHERALS

Peripherals #	Connection interval ms	Notification rate Hz
1	7.5	~1000
4	30	200
8	60	50

normal running mode with BLE activated, which results in a relatively high power consumption of 133.5 mW on average. However, this mode is executed only at the first sensor node connection or after a hardware reset. Once the BLE connection is established, the sensor node transfers to the *sleep stage*, where the MCU switches to the stop mode (deep low-power state supported by the STM32L4 family) with all the sensors and the frontend powered off. In the *sleep stage*, the power consumption of the MCU is 24.30  $\mu$ W on average, in addition to the BLE module that needs 3  $\mu$ W. An internal low-power timer wakes up the MCU from the stop mode every 4 seconds, which moves the STWIN from the *sleep stage* to a *measuring stage*. The *measuring stage* starts with powering on the frontend, followed by a 200 ms delay to fully activate the circuitry ( $t_{on}$ ), which needs 29.11 mJ of energy. Then a calibration of the ADC is performed, which consumes 25.83 mJ of energy in 141 ms. Then, in the *data acquisition stage*, 100 data samples are acquired and processed at a sampling rate of 1000 Hz, costing 19.63 mJ of energy in 104 ms. After the acquisition, the frontend and the UART communication are powered off. After the onboard processing, executed in conjunction with the acquisition, the calculated corona current value, as well as device information data including environmental information, battery status, etc., is transmitted via BLE, where 5.92 mJ of energy is consumed in 36 ms. At last, the platform switches to stop mode.

The overall characteristic of the sensor node power consumption is summarized in Table IV. As presented, over 80 % of the energy in a working cycle is consumed in the calibration acquisition and onboard processing. Thus, a small amount of energy is used to transmit the data.

Based on the power consumption characteristic, we can thereby calculate the expected lifetime of the battery, as expressed in Eq. (3). The valid duration of a working cycle is about 500 ms. Assuming the duty cycle of the platform is  $D$ , then the energy consumption in one cycle is given by (including the working cycle and the idle stage) Eq. (1), where  $P$  indicates the mode power and  $t$  its expected time. Subscripts  $s, f, c, a, on$ , and TX indicate idle, frontend, calibration, acquisition, power on, and transmission respectively. In our case, the energy consumption in a valid working cycle is 55.93 mJ, and the power consumption in the idle stage is 27.3  $\mu$ W, by which the expected lifetime of a battery can be thereby given in Eq. (3), which result is in seconds.

$$E_{\text{cycle}} = P_s \cdot t_s + P_f(t_{on} + t_c + t_a) + P_c \cdot t_c + P_a \cdot t_a + P_{\text{TX}} \cdot t_{\text{TX}}, \quad (1)$$

TABLE IV  
POWER CONSUMPTION IN A WORKING CYCLE

	Sleep	Frontend	Measurement		Transmission
			Calibration	Acquisition*	
Power / mW	0.027	8.07	183.19	188.75	164
Energy / mJ	-	4.55	25.83	19.63	5.92
Proportion	-	8.14%	46.18%	35.10%	10.58%

\*Onboard processing is included

$$t_{\text{cycle}} = t_s + t_{on} + t_c + t_a + t_{\text{TX}} = \frac{0.5 \text{ s}}{D}, \quad (2)$$

$$t_{\text{battery}} = \frac{E_{\text{battery}}}{E_{\text{cycle}}} \cdot t_{\text{cycle}}. \quad (3)$$

In our test setup, the duty cycle  $D$  is 12.5 %. Then the energy consumption in one cycle is 55.94 mJ, which means that 52.9 days are expected from a 3.7 V / 4800 mAh battery (17.76 J). By decreasing the duty cycle to 1 %, equivalent to one measurement every 50 s, the expected lifetime of the same battery can be increased to 1.8 years.

## IV. MEASUREMENT RESULTS

### A. Our experimental setups

Our indoor laboratory offers the possibility to hang a 6 m section of overhead line under a rain simulator, providing repeatable and controlled test conditions. The conductor is placed between two large toroids (that can influence the absolute value of the electric field) at a height of 2.5 m with minimal sag. Both conductors tested have a diameter of 22.4 mm, which energized at 185 kV DC yields an electric field gradient of 27.25 kV/cm at the conductor surface.

Outdoors, in a completely uncontrolled environment subject to real weather conditions, we use a 10 m long  $-60$  kV negative DC test line. The conductor is a 34-AL3 AAAC 7 strands conductor with a 7.5 mm diameter hanging at 1.2 m above ground at its lowest sag, which corresponds to a gradient at the conductor surface of 24.8 kV/cm.

### B. Conductors comparison

Our sensor platform can be benchmarked by its ability to compare the corona behavior of different conductors during wet weather transitions. Indeed, both microscopic [29] and macroscopic [30] conductor properties define corona performance in rain. The examined conductors differ in their surface properties, their wettability, as well as the water droplet formation and distribution on their surface.

Fig. 5 shows the simultaneous progression of signals from all three of our sensors over time comparing a new conductor (darker-colored plot lines) and an aged conductor (lighter-colored plot lines). The corona current is shown in blue at the top, the electric field at ground level as measured by the field mill in orange, and the ion current density at ground level in green at the bottom. While the corona current is measured for the entire length of the conductor, the electric field and ion current density measurements are localized to where the respective sensors are placed. As the corona discharges influence the electromagnetic environment not only right below the

line but along the entire right of way corridor (a few meters wide and parallel to the line) as well, both sensors are placed 2.5 m off the axis of the conductor.

Before the line is energized, all sensors show 0. As voltage is applied, the space charge free electrostatic field (Laplace field) rises to the same value of around 17 kV/m for both conductors (Fig. 5 instants A to B). Here, the setup does not exhibit dry corona as shown by the corona current and ion current at ground level remaining null. While rain is applied on the line at the same rain rate of approximately 4 mm/h for both conductors (instants B to C), all three quantities first increase rapidly, then more slowly towards a wet steady state that is reached in around 15 minutes after the rain started. It is evident that the new conductor produces significantly more corona than the aged one when wet.

Some of the water droplets on the conductors act as corona sources. Those corona sources cause an ion current that can be measured as the total corona current flowing through the line or an ion current density at ground level through the area of our Wilson plate. Moreover, the presence of free charge carriers in the air between the line and ground modifies the electric field, adding a space charge field component (Poisson field).

As rain ceases (instant C), both conductors start to dry off and corona levels decrease. The ways in which both conductors dry show significant differences as well. Shortly before instant D, the rate at which corona activity decreases on the new conductor accelerates again before completely drying out. The aged conductor will go on at a more or less constant level of corona activity for over 5 more hours before drying out. This phase is not shown here for clarity. It should be noted that acoustic emissions from the lines were audible whenever the corona current was above zero.

The lower corona current measured for the aged conductor during the wet state (instants B to C) can be explained by the lower number of water droplets on its surface. Thus, fewer discharges occur compared to the new conductor. The aged conductor also shows a clear difference in the drying behavior (instants C to D). Due to the strong hydrophilic properties of the surface, a non-coronating water film is formed that “feeds” the few coronating water droplets long after the rain stops. For this reason, the drying phase is much longer for the aged conductor than for the new one without the hydrophilic properties where the droplets eventually dry out.

At the 12 minutes mark, a small peak of dry corona (probably a dust particle on the line) is visible for the new conductor measurements of the corona current and the electric field but not for the Wilson plate. This is a consequence of the localized nature of the bottom two sensors and shows a benefit of monitoring different corona effects on the same line.

Our platform allows to distinguish both conductors based on their corona performance during wet weather transitions. All three measured quantities give different insights into the behavior and provide a fuller picture of the process than if only one of the parameters were measured.

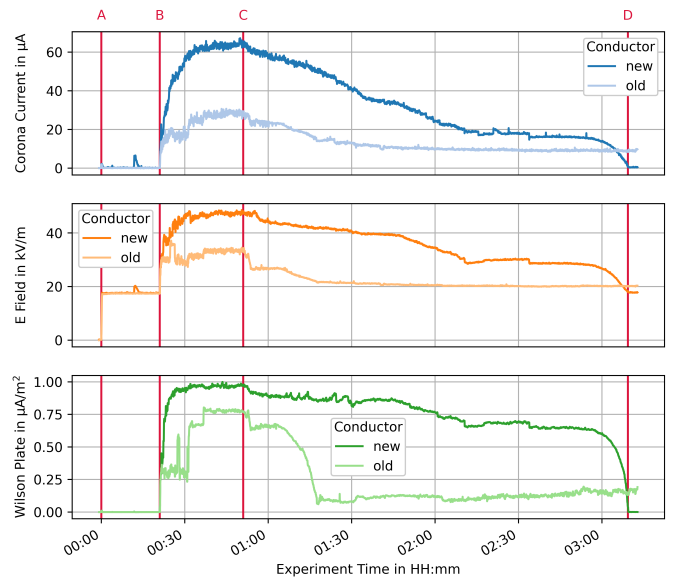


Fig. 5. Two measurements showing the corona behavior of two different conductors in corresponding fair weather, rain, and drying phases. The vertical lines respectively show the time instants when (A) the originally dry and grounded line was energized to 185 kV, (B) the rain started pouring on the line, (C) rain ceased, and (D) the new conduction was fully dry again. The darker-colored plot lines are from a new conductor, and the lighter ones are from an aged conductor.

### C. Possible representations of highly dynamic signals

This section presents and discusses an outdoor measurement to illustrate some of the possibilities offered by the features of our platform. Fig. 6 shows over 4 hours of an ion current measurement made with a Wilson plate sensor.

The sensor samples data at a frequency  $f_s = 250$  Hz. When performing long-term measurements to observe how the ion current is related to weather phenomena (which have time constants in the order of minutes), it wouldn't be practical to continuously record data at this rate. Thus, ten times per minute, the sensor records data during a sampling interval of  $T_{SI} = 3$  s (still at  $f_s = 250$  Hz), processes those raw samples and sends out a statistic describing the sampling interval. Deciding on what statistic to transmit instead of the raw data of every single sample is a balancing act between data throughput, energy consumption and storage, and the scientific value of the collected data. The bottom three plots in Fig. 6 show different kinds of statistics displayed as sent by the sensor node without further post-processing.

Unlike in indoor measurements, outdoors, wind can add or remove water droplets as well as dry particles to the line that can all potentially act as corona sources. The time delay observed between the two rain onsets of the snapshot in Fig. 6 and a corresponding increased corona activity could be attributed to the time it takes for water percolating around this small radius conductor to form coronating droplets. Collecting larger amounts of data using this sensor platform shall enable us to be more conclusive about such assumptions.

In the second, the mean of the measured signal is the dark blue line, while the lighter blue lines show the extent of the minimum and maximum value within a given sampling



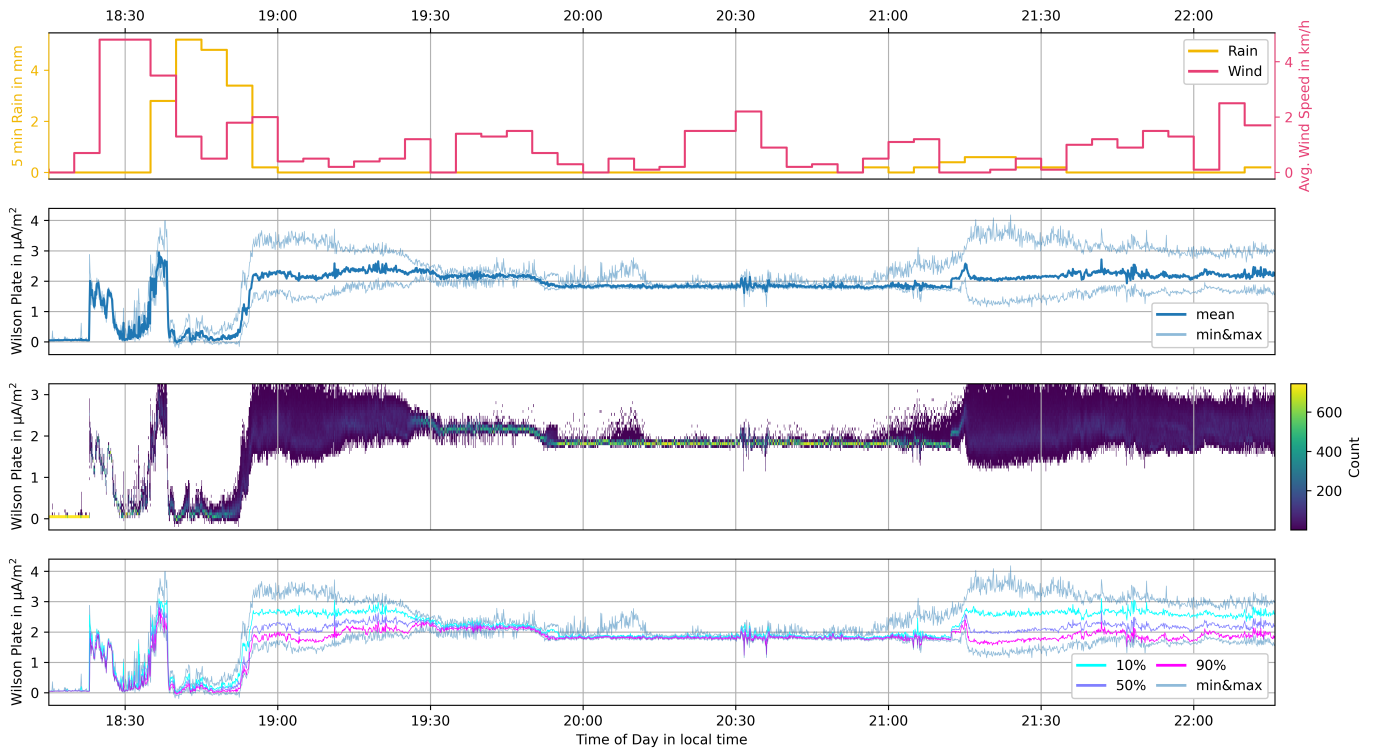


Fig. 6. Weather data along with three different statistics representing the same ion current data as computed and sent out by one of our sensor nodes. The weather data shows rain precipitation in mm/h and the average wind speed in km/h with a 5 minutes resolution. The second plot shows the min mean and max of the signal. The third figure shows a 2D histogram of the data with fixed bins. The bottom plot shows quantiles of the measured data along the min and max.

interval  $T_{SI}$ .

The following figure shows a 2D histogram of the ground-level ion current density during the same time period. Each horizontal bin is a sampling interval  $T_{SI}$  and there are 50 vertical bins covering the range shown on the y-axis (the entire measurement range of the sensor is not shown here for clarity). The color indicates how many samples (count) of a given amplitude (y-axis) were captured within each sampling interval  $T_{SI}$  after 21:00. The max line deviating from the mean happens to correspond with rain activity picking up again at 21:00 after a 2 hour pause. What remains unclear is whether the peaks are sharp and isolated or broader and/or more frequent while allowing the mean to stay relatively constant.

The bottom plot shows different quantiles of all samples measured within each single sampling interval  $T_{SI}$ . Specifically, the median of the data as the 50% quantile, the 10% quantile (the lines above which lie 10% of the data points from a sampling interval or reciprocally below which lie 90% of the data) and the 90% quantile. Additionally, the minimum and maximum are shown in the top plot to indicate the full extent within which samples were measured.

The top plot requires 3 float numbers per sampling interval  $T_{SI}$ . The middle image requires 50 integers per sampling interval while the lower plot requires 5 floats for the quantiles, the minimum and the maximum.

Firstly, looking at the top plot, it is evident that transmitting only the mean value of every sampling interval  $T_{SI}$  would not be sufficient to represent the signal faithfully. Indeed, for

instance, while considering only the dark blue line between 20:15 and 20:30, and between 21:00 and 21:15, one might be under the impression that the signal is very similar for both time intervals. The minimum and maximum lines already allow us to observe that the signal must have been much more dynamic during the second time interval than the first. They suggest that ion current peaks occur within each sampling interval  $T_{SI}$  after 21:00. The max line deviating from the mean happens to correspond with rain activity picking up again at 21:00 after a 2 hour pause. What remains unclear is whether the peaks are sharp and isolated or broader and/or more frequent while allowing the mean to stay relatively constant.

The middle heatmap, gives an easy but detailed visual representation of the data spread. Values are indeed concentrated around the mean between 19:30 and 21:15, with only occasional excursions towards extreme values. Between 18:15 and 19:30 or after 21:15, on the contrary, the values are spread around the entire range between the minimum and maximum recorded values for the given sampling intervals  $T_{SI}$ . As rain sets in around 21:00 and the max value starts diverging from the mean value, the heat map confirms that it is only 15 minutes later, beginning at 21:15, that the spread in sampled data points within a sampling interval  $T_{SI}$  becomes significant. After that time, this central figure becomes more difficult to read.

Here, the bottom plot provides deeper insights than the other plots could. For instance, between 21:15 and 22:00, the max plot line decreases steadily, but the 10% line remains relatively

flat, indicating that 90% of the data points remain under a fixed threshold. During the same period, it is also notable that the spacing between the quantiles is relatively large and becomes narrower as time passes by, starting around 21:45. While the max values seem to start decreasing as soon as the rain ceases, the narrowing of the quantiles seems to happen later during the drying of the overhead line. With these results, we show how long-term measurement campaigns can improve the characterization of the corona behavior on overhead lines under varying weather conditions.

It should also be noted that those processing capabilities allow tight integration of the wireless transmission and low-power features mentioned above. It is easy to imagine scenarios in which such interactions could be leveraged to further enhance the performance of our sensor nodes. For instance, during a long-term measurement, the sensor node could receive commands to adapt measurement parameters (such as sampling rate and period) dynamically based on weather forecast reports, thus avoiding excessive data collection at times when no significant corona activity is expected. However, to ensure that unforeseen events are correctly recorded, the sensor node could still decide to adapt measurement parameters independently based on onboard logic.

## V. OUTLOOK

The sensor platform presented in this paper has been explicitly developed to be modular and easily extensible. Many other corona-related effects could be quantified using this platform, one of the most important of which is audible noise emissions. Traditionally those have been difficult to capture accurately, especially in outdoor settings, since ambient noises are also often present. Our platform's wireless and low-power capabilities enable sensors to be placed in very close proximity to the lines themselves (under high potential). This, of course, would permit the recording of acoustic emissions from the corona with a far better signal-to-noise ratio than if done from the ground.

Another example would be the measurement of the line voltage local to where corona is being monitored on the grid. Indeed, on large grids, unlike on short test lines, the Ferranti effect or the harmonic distortion of the voltage might impact corona behaviour and the voltage would need to be measured on site and not just at the power source.

The relative low cost and scalability of the platform also make potential large deployments a more realistic prospect. Both in the sense of several ground-based sensors in a line perpendicular to the overhead conductor to cross-section profiles, and in that of a wide range of geographic locations subjected to different environmental conditions. This shall help grid operators know if the seasonal variations in corona performance observed in one region also applies in another. The larger the dataset, the better predictions will be when it comes to planing new lines.

It should also be noted that this sensor platform is presented in the context of increased interest in Wireless Sensor Networks (WSN) for smart grids [32], [33], where it could potentially be of interest.

Even in its current state, such a platform allows an easier and more thorough characterization of the corona performance of different conductors as demonstrated with our first application example. This not only helps grid planners select the best conductors for their use case, but will also help conductor manufacturers in bringing innovations to the market.

## VI. CONCLUSION

This paper introduces current research questions on the corona effects around high voltage overhead lines. After introducing how IoT technologies are useful in this context, we presented a unified sensor platform based on those technologies. To the authors' knowledge, it constitutes the first time that three different corona-related quantities are measured by a unified platform, namely (i) the corona current through the line, (ii) the ground level electric field, (iii) and the ground level ion current density.

Proof of concept indoor measurements are then presented. They show that results from the three different sensors measuring three related but distinct physical quantities match expectations. Those measurements also demonstrate the platform's ability to distinguish between conductor types having different corona performances.

Lastly, we show real outdoor measurements. Thanks to the onboard processing capabilities, low energy consumption and high reliability of our sensors, long-term data of up to several months can be represented in innovative ways that not only might help determine trends and patterns but that are also more practical from a data acquisition and handling point of view.

## ACKNOWLEDGMENTS

This work is partially funded by the BRIDGE Discovery Programme of the Swiss National Science Foundation and Innosuisse, project number 40B2 – 0\_187087 and the German TSO TransnetBW GmbH. Rainer Pürzelmayr and Kilian Schillai helped by providing material samples. Fabian Mächler, Kamil Halvdan Dwinger and, Simon Hauri supported the construction of the test setups. Moreover, the authors thank Fabian Ulmer, Sergio Meyer, and Jackie Lim for their practical contribution to this work.

## REFERENCES

- [1] Y. Saleem, N. Crespi, M. H. Rehmani, and R. Copeland, "Internet of things-aided smart grid: Technologies, architectures, applications, prototypes, and future research directions," *IEEE Access*, vol. 7, pp. 62 962–63 003, 2019.
- [2] S. Ahmadzadeh, G. Parr, and W. Zhao, "A review on communication aspects of demand response management for future 5g iot-based smart grids," *IEEE Access*, vol. 9, pp. 77 555–77 571, 2021.
- [3] S. Hedtke, P. Bleuler, and C. Franck, "Outdoor investigation of the corona characteristics and audible noise of a hybrid ac/dc overhead line," *IEEE Transactions on Power Delivery*, vol. 36, no. 6, pp. 3309–3317, 2020.

- [4] J.-R. Riba, A. Gomez-Pau, and M. Moreno-Eguilaz, "Sensor comparison for corona discharge detection under low pressure conditions," *IEEE Sensors Journal*, vol. 20, no. 19, pp. 11 698–11 706, 2020.
- [5] Q. Wang, D. Kundur, H. Yuan, Y. Liu, J. Lu, and Z. Ma, "Noise suppression of corona current measurement from hvdc transmission lines," *IEEE Transactions on Instrumentation and Measurement*, vol. 65, pp. 264–275, 2 Feb. 2016.
- [6] R. M. Morris, A. Staniforth, and A. R. Morse, "A data system for high-voltage dc test lines," *IEEE Transactions on Instrumentation and Measurement*, vol. IM-20, pp. 285–291, 4 Nov. 1971.
- [7] V. L. Chartier and R. Stearns, "Formulas for predicting audible noise from overhead high voltage ac and dc lines," *IEEE Transactions on Power Apparatus and Systems*, vol. PAS-100, pp. 121–130, 1 Jan. 1981.
- [8] N. Davari, G. Akbarizadeh, and E. Mashhour, "Intelligent diagnosis of incipient fault in power distribution lines based on corona detection in uv-visible videos," *IEEE Transactions on Power Delivery*, vol. 36, no. 6, pp. 3640–3648, 2020.
- [9] M. G. Comber and R. Nigbor, "Audible noise performance of the first three-phase ultra-high voltage transmission test line at epri's project uhv," *IEEE Transactions on Power Apparatus and Systems*, vol. 95, pp. 1105–1114, 4 1976.
- [10] J. Lundquist, "Methods for predicting ac transmission line audible noise by short-term single-pahse tests," *IEEE Transactions on Power Apparatus and Systems*, vol. PAS-103, pp. 283–293, 2 Feb. 1984.
- [11] D. E. Perry, V. L. Chartier, and G. L. Reiner, "Bpa 1100 kv transmission system development corona and electric field studies," *IEEE Transactions on Power Apparatus and Systems*, vol. PAS-98, pp. 1728–1738, 5 Sep. 1979.
- [12] EPRI, *EPRI AC Transmission Line Reference Book - 200 kV and Above, Third Edition*, 3rd. 2005, pp. 1–1074.
- [13] K. Y. Shin, J. A. Oh, G. M. Kwon, M. N. Ju, and J. M. Woo, "Long-term evaluation of hvdc transmission line audible noise and its correlation with background noise," *AIP Advances*, vol. 9, p. 095 014, 9 Sep. 2019.
- [14] S. Hedtke, M. Pfeiffer, M. Gobeli, P. Bleuler, R. Bräunlich, and C. M. Franck, "Setup of an outdoor hybrid ac / dc test line for corona measurements," 2018.
- [15] P. Wang and G. Zhang, "The measurement method for corona discharge current under high-voltage environment," *IEEE Transactions on Instrumentation and Measurement*, vol. 57, pp. 1786–1790, 8 Aug. 2008.
- [16] A. J. Thomas, I. C. and C. C. Reddy, "A method for surface voltage measurement of an overhead insulated conductor," *IEEE Transactions on Instrumentation and Measurement*, vol. 70, pp. 1–8, 2021.
- [17] O. M. Butt, M. Zulqarnain, and T. M. Butt, "Recent advancement in smart grid technology: Future prospects in the electrical power network," *Ain Shams Engineering Journal*, vol. 12, no. 1, pp. 687–695, 2021.
- [18] H. Kudyan and C. H-Shih, "A nonlinear circuit model for transmission lines in corona," *IEEE Transactions on Power Apparatus and Systems*, vol. PAS-100, pp. 1420–1430, 3 Mar. 1981.
- [19] H. Liu, Q. Zhang, Y. Luo, J. Wu, and X. Bai, "Feasibility study of metalized membrane method applied to monitoring corona loss of ac/dc transmission line," in *2011 1st International Conference on Electric Power Equipment-Switching Technology*, IEEE, 2011, pp. 253–257.
- [20] C. R. Paul, *Introduction to electromagnetic compatibility*. John Wiley & Sons, 2006.
- [21] A. Alassi, S. Bañales, O. Ellabban, G. Adam, and C. MacIver, "HVDC Transmission: Technology Review, Market Trends and Future Outlook," *Renewable and Sustainable Energy Reviews*, vol. 112, pp. 530–554, Sep. 2019.
- [22] Übertragungsnetzbetreiber, "Netzentwicklungsplan Strom 2035," Tech. Rep., 2021.
- [23] IEEE, "IEEE guide for the measurement of dc electric-field strength and ion related quantities," 1990.
- [24] Q. Yang, R. Liu, Y. He, and M. Luo, "Ac/dc hybrid electric field measurement method based on pockels effect and electric field modulation," *Review of Scientific Instruments*, vol. 91, p. 055 004, 5 May 2020.
- [25] Y. Cui, H. Yuan, X. Song, L. Zhao, Y. Liu, and L. Lin, "Model, design, and testing of field mill sensors for measuring electric fields under high-voltage direct-current power lines," *IEEE Transactions on Industrial Electronics*, vol. 65, pp. 608–615, 1 Jan. 2018.
- [26] M. G. Comber and G. Johnson, "Hvdc field and ion effects research at project uhv: Results of electric field and ion current measurements," *IEEE Transactions on Power Apparatus and Systems*, vol. PAS-101, pp. 1998–2006, 7 Jul. 1982.
- [27] J. A. Chalmers, "The measurement of the vertical electric current in the atmosphere," *Journal of Atmospheric and Terrestrial Physics*, vol. 24, pp. 297–302, 4 1962.
- [28] C. Fang, X. Cui, X. Zhou, T. Lu, Y. Zhen, and X. Li, "Impact factors in measurements of ion-current density produced by high-voltage dc wire's corona," *IEEE Transactions on Power Delivery*, vol. 28, pp. 1414–1422, 3 Jul. 2013.
- [29] C. Stamatopoulos, P. Bleuler, M. Pfeiffer, S. Hedtke, P. R. von Rohr, and C. M. Franck, "Influence of surface wettability on discharges from water drops in electric fields," *Langmuir*, vol. 35, pp. 4876–4885, 14 Apr. 2019.
- [30] H. Kirchner and C. M. Franck, "B2 ps3 11145 correlation of the surface wettability and the audible noise emission of overhead line conductors," 2022.
- [31] P. Bleuler, S. Hedtke, and C. Franck, "Corona performance of dc overhead lines in outdoor experiments during wet weather transitions and under varying humidity," *CIGRE Digital-E-Session 2020: Papers and Proceedings*, 2020.



- [32] E. Fadel, V. Gungor, L. Nassef, *et al.*, “A survey on wireless sensor networks for smart grid,” *Computer Communications*, vol. 71, pp. 22–33, Nov. 2015.
- [33] I. Kouveliotis-Lysikatos, N. Hatzigargyriou, Y. Liu, and F. Wu, “Towards an internet-like power grid,” *Journal of Modern Power Systems and Clean Energy*, 2020.



**Pascal Bleuler** studied electrical engineering at EPFL (Switzerland) with a stay at the University of Bologna (Italy). In 2017 he officially joined the High Voltage Laboratory (HVL) at ETH Zürich (Switzerland) after collaborating with it during a year, investigating the deformation of water droplets in electric fields and related partial discharge mechanisms. In 2023 he received the Dr. sc. degree from ETH Zürich for his research on outdoor HVDC overhead corona over long time periods.



**Tommaso Polonelli** (M'20) received the M.Sc. degree and the Ph.D. in electronics engineering from the University of Bologna, Bologna, Italy, in 2017 and 2020, respectively. He is currently a Lecturer and post-doctoral researcher at ETH Zürich, Zürich, Switzerland. His research work focuses on wireless sensor networks, IoT, autonomous unmanned vehicles, power management techniques, structural health monitoring, and the design of ultra-low power battery-supplied devices with onboard intelligence. He has collaborated with several universities and

research centers, such as the University College Cork, Cork, Ireland, and the Imperial College London, London, U.K. He has authored over 30 papers in international journals and conferences.



**Yu Xiao** received the B.Sc. degree and Ph.D. degree in Electrical Engineering from Xi'an Jiaotong University, Xi'an, China, in 2017 and 2023, respectively. Currently, he is a postdoctoral researcher at TU/e, Eindhoven, Netherlands.

His research interests are mainly in the field of power electronics, protection and control of MVDC power systems, high-capacity DC breaking, and IoT-based predictive maintenance. From 2021 to 2022, he was with the Swiss Federal Institute of Technology (ETH) Zurich, Zurich, Switzerland, as a visiting scholar, where his work focused on wireless sensor networks and power consumption optimization.



**Benjamin Stadler** is currently studying at ETH Zürich. He obtained a B.Sc. in 2022, contributing to this publication with his bachelor thesis and as an employee of the High Voltage Lab.



**Lorenz Gallina** is currently a software engineer for Swiss energy supply companies. He received the M.Sc. degree in Electrical Engineering at ETH Zürich, Zürich, Switzerland, in 2022. His master's thesis and semester thesis focused on the use of IoT devices to investigate corona currents on overhead lines.



**Hannah Kirchner** received the Diploma degree in electrical engineering from the Technical University of Dresden, Dresden, Germany, in 2019. From 2019 to 2020, she was with the Pfiffner Messwandler AG in Hirschthal, Switzerland as a test engineer at the high voltage laboratory. Currently, she is a doctoral student at the Swiss Federal Institute of Technology (ETH) Zurich, Zurich, Switzerland. Her research work focuses on noise emission of overhead lines due to corona discharges.



**Michele Magno** is currently a Senior Scientist at ETH Zürich, Switzerland, at the Department of Information Technology and Electrical Engineering (D-ITET). Since 2020, he is leading the D-ITET center for project-based learning at ETH. He received his master's and Ph.D. degrees in electronic engineering from the University of Bologna, Italy, in 2004 and 2010, respectively. He is working in ETH since 2013 and has become a visiting lecturer or professor at several universities, namely the University of Nice Sophia, France, Enssat Lannion, France,

University of Bologna and Mid University Sweden, where currently is a full visiting professor at the electrical engineering department. His current research interests include smart sensing, low-power machine learning, wireless sensor networks, wearable devices, energy harvesting, low-power management techniques, and extension of the lifetime of batteries-operating devices. He has authored more than 220 papers in international journals and conferences. He is a senior IEEE member and an ACM member. Some of his publications were awarded as best papers awards at IEEE conferences. He also received awards for industrial projects or patents.



**Christian M. Franck** (Senior Member, IEEE) received the Diploma degree in physics from the University of Kiel, Kiel, Germany, in 1999, and the Ph.D. degree in physics from the University of Greifswald, Greifswald, Germany, in 2003.

From 2003 to 2009, he was with the ABB Swiss Corporate Research Center, Baden, Dättwil, Switzerland, as a Scientist and a Group Leader for gas circuit breakers and high-voltage systems. He is currently a Full Professor of high-voltage technology with the Swiss Federal Institute of Technology (ETH) Zürich, Zürich, Switzerland. His current main research interests include gaseous and solid insulation systems, switching arcs and power line corona.